

# Porous ultrathin-shell microcapsules designed by microfluidics for selective permeation and stimuli-triggered release

Li Chen<sup>1,2,3</sup>, Yao Xiao<sup>2</sup>, Zhiming Zhang<sup>2</sup>, Chun-Xia Zhao<sup>4</sup>, Baoling Guo (✉)<sup>1</sup>,  
Fangfu Ye (✉)<sup>3,5</sup>, Dong Chen (✉)<sup>2,6</sup>

<sup>1</sup> Department of Oncology, Longyan First Affiliated Hospital of Fujian Medical University, Longyan 364000, China

<sup>2</sup> Zhejiang Key Laboratory of Smart Biomaterials, College of Chemical and Biological Engineering, Zhejiang University, Hangzhou 310027, China

<sup>3</sup> Wenzhou Institute, University of Chinese Academy of Sciences, Wenzhou 325001, China

<sup>4</sup> Faculty of Engineering, Computer, and Mathematical Sciences, The University of Adelaide, Adelaide, SA 5005, Australia

<sup>5</sup> Beijing National Laboratory for Condensed Matter Physics, Institute of Physics, Chinese Academy of Sciences, Beijing 100190, China

<sup>6</sup> College of Energy Engineering and State Key Laboratory of Fluid Power and Mechatronic Systems, Zhejiang University, Hangzhou 310027, China

© Higher Education Press 2022

**Abstract** Microcapsules are versatile delivery vehicles and widely used in various areas. Generally, microcapsules with solid shells lack selective permeation and only exhibit a simple release mode. Here, we use ultrathin-shell water-in-oil-in-water double emulsions as templates and design porous ultrathin-shell microcapsules for selective permeation and multiple stimuli-triggered release. After preparation of double emulsions by microfluidic devices, negatively charged shellac nanoparticles dispersed in the inner water core electrostatically complex with positively charged telechelic  $\alpha,\omega$ -diamino functionalized polydimethylsiloxane polymers dissolved in the middle oil shell at the water/oil interface, thus forming a porous shell of shellac nanoparticles cross-linked by telechelic polymers. Subsequently, the double emulsions become porous microcapsules upon evaporation of the middle oil phase. The porous ultrathin-shell microcapsules exhibit excellent properties, including tunable size, selective permeation and stimuli-triggered release. Small molecules or particles can diffuse across the shell, while large molecules or particles are encapsulated in the core, and release of the encapsulated cargos can be triggered by osmotic shock or a pH change. Due to their unique performance, porous ultrathin-shell microcapsules present promising platforms for various applications, such as drug delivery.

**Keywords** microcapsule, emulsion, microfluidics, selective permeation, stimuli-triggered release

## 1 Introduction

Microcapsules with hierarchical core-shell structures are versatile delivery vehicles and are often used to encapsulate active ingredients, such as nutrients, fragrances, biomolecules and medicines, for long-term storage and controlled release [1–4]. Traditional microcapsules generally contain a solid shell and possess some common features, including (i) high loading efficiency to ensure maximum utilization of expensive and rare ingredients [5–7], (ii) tunable size for desired purposes [8–10] and (iii) long-term storage to protect active ingredients from degradation [11,12]. The design and functionalization of the shell could further endow the microcapsules with diverse functionalities. For example, when the microcapsule shell is biodegradable, active ingredients could be released sustainably for a long period of time upon degradation or undergo rapid stimuli-triggered release under suitable conditions [13–16]. Despite these advances, microcapsules featuring selective permeation and multiple modes of stimuli-triggered release are still rare and challenging.

Microfluidics, which allows precise control of the hierarchical structures of emulsions, provides a versatile platform for design and preparation of microcapsules with desired structures and properties [17–19]. For example,

Received March 30, 2022; accepted May 24, 2022

E-mails: baolingguo@sina.com (Guo B.), fye@iphy.ac.cn (Ye F.), chen\_dong@zju.edu.cn (Chen D.)

monodisperse core-shell double emulsions can be precisely generated in microfluidic channels in one step [20–22], and these could be used as templates for design and preparation of microcapsules in which the properties of the shell could be tuned. While double emulsions are generally unstable and fail in long-term stabilization [23], microcapsules are able to encapsulate cargos for long-term storage. A common strategy used to turn double emulsions into microcapsules is to dissolve polymers in the middle oil phase, and a solid polymeric shell is formed upon evaporation of the middle oil phase [24–26]. However, microcapsules with solid shells generally do not support selective permeation and only possess a simple release mode. Therefore, innovations and novel strategies are required for design and preparation of microcapsules with desired properties and functionalities to meet growing needs.

Here, we design and prepare porous ultrathin-shell microcapsules using ultrathin-shell water-in-oil-in-water (W/O/W) double emulsions as templates. W/O/W double emulsions are first prepared by using a glass capillary microfluidic device. Due to electrostatic interactions, negatively charged shellac nanoparticles (NPs) dispersed in the inner water core automatically complex with a positively charged telechelic  $\alpha,\omega$ -diamino functionalized polydimethylsiloxane ( $\text{NH}_2$ -PDMS- $\text{NH}_2$ ) polymer dissolved in the middle oil shell at the water/oil interface. Moreover, telechelic  $\text{NH}_2$ -PDMS- $\text{NH}_2$  molecules with two amino end groups bridge neighboring shellac NPs, thus forming a cross-linked network. Therefore, porous ultrathin-shell microcapsules are achieved upon evaporation of the middle oil phase. The microcapsule size can be tailored by tuning the flow rate of the outer phase. Selective permeation allowing small molecules or particles to diffuse across the microcapsule shell is demonstrated, the while large molecules or particles are stably encapsulated in the core. The microcapsules could rupture under osmotic shock or disintegrate in response to a pH change, thereby enabling multiple stimuli-triggered releases.

## 2 Experimental

### 2.1 Materials

Shellac is a natural resin and was purchased from Sigma-Aldrich (USA). Shellac was first dissolved in ethanol and then precipitated to form NPs upon rapid mixing of ethanol with water. Due to the carboxylic groups on the surface, shellac NPs are negatively charged and well dispersed in the inner water phase. *n*-Hexane was purchased from Sinopharm Group Chemical Reagent Co., Ltd. (China), and  $\text{NH}_2$ -PDMS- $\text{NH}_2$  with a molecular weight of  $M_w = 25000 \text{ g}\cdot\text{mol}^{-1}$  was purchased from

Gelest Inc. (USA).  $\text{NH}_2$ -PDMS- $\text{NH}_2$  dissolved in *n*-hexane was used as the middle oil phase. Polyvinyl alcohol (PVA, 87%–89% hydrolyzed) was purchased from Sigma-Aldrich (USA) and dissolved in the outer water phase, and this served as the surfactant. Water-soluble red ink (KST-LM) was purchased from Dayuan Office Group Co., Ltd. (China). Oil-soluble Nile red was purchased from Shanghai Yuanye Bio-Technology Co., Ltd. (China). Rhodamine B was obtained from Macklin Biochemical Co., Ltd. (China). Hydroxy-terminated poly(L-lactic acid) (PLLA) with a molecular weight of  $M_w = 3000 \text{ g}\cdot\text{mol}^{-1}$  was purchased from Jinan Daigang Biomaterials Company (China). Sodium hydroxide (NaOH, purity 96%) was purchased from Sinopharm Group Chemical Reagent Co., Ltd. (China). Polyethylene glycol (PEG) with a molecular weight of  $M_w = 6000 \text{ g}\cdot\text{mol}^{-1}$  was purchased from Macklin Biochemical Co., Ltd.

### 2.2 Preparation of shellac NPs

First, 50 mg of shellac was first dissolved in 1 mL of ethanol. A 100  $\mu\text{L}$  solution of shellac in ethanol was rapidly injected into 3 mL of deionized water via a gel-loading pipet tip and then shaken for 60 s. Upon rapid mixing of the ethanol with water, shellac precipitated to form NPs. The average size of the shellac NPs was  $D \approx 100 \text{ nm}$ , and the zeta potential was  $\zeta \approx -40 \text{ mV}$ , as measured by a Zetasizer (Nano ZSP, Malvern Instruments, UK). Due to the carboxylic groups on the surface, shellac NPs were negatively charged and well dispersed in the inner water phase.

### 2.3 Preparation of porous ultrathin-shell microcapsules using ultrathin-shell double emulsions as templates

Ultrathin-shell W/O/W double emulsions were prepared by using a glass capillary microfluidic device. The cylindrical glass capillaries have an inner diameter of 0.55 mm and an outer diameter of 0.96 mm. Square glass capillaries have an inner diameter of 1.01 mm and an outer diameter of 1.5 mm. Cylindrical glass capillaries were tapered by using a micropipette puller (Model-P1000, Sutter Instrument Co., Ltd., USA), and their nozzles were then sanded into the desired size. The nozzle diameters of the inner, middle and outer capillaries were 20, 180 and 340  $\mu\text{m}$ , respectively. To assemble the microfluidic device, the inner capillary was inserted into the middle capillary, and the middle and outer capillaries were aligned face-to-face with a separation of  $\sim 300 \mu\text{m}$  in a square capillary. Syringe pumps (LSP01-1A, Longer, China) were used to pump liquid phases into the devices with constant flow rates.

To make ultrathin-shell W/O/W double emulsions, 1.7  $\text{mg}\cdot\text{mL}^{-1}$  shellac NPs dispersed in water were used as

the inner aqueous phase, 1 wt %  $\text{NH}_2\text{-PDMS-NH}_2$  dissolved in *n*-hexane was used as the middle oil phase, and 5 wt % PVA dissolved in water was used as the outer aqueous phase. Ultrathin-shell double emulsions were generated with constant flow rates of 200, 400 and 10000  $\mu\text{L}\cdot\text{h}^{-1}$  for the inner, middle and outer phases. Since shellac NPs are negatively charged and  $\text{NH}_2\text{-PDMS-NH}_2$  molecules are positively charged, shellac NPs and  $\text{NH}_2\text{-PDMS-NH}_2$  molecules electrostatically complexed with each other at the water/oil interface [27,28]. Moreover, the  $\text{NH}_2\text{-PDMS-NH}_2$  molecules contain two amino end groups and were able to bridge neighboring shellac NPs, thus forming a cross-linked network. When *n*-hexane was evaporated after 24 h, ultrathin-shell double emulsions became porous ultrathin-shell microcapsules.

#### 2.4 Characterization of porous ultrathin-shell microcapsules

Porous ultrathin-shell microcapsules were observed with a bright-field optical microscope (CX40P, Sunny Optical Technology Co., Ltd., China), and fluorescent images were taken with a fluorescence confocal microscope (TCS SP5, Leica, Germany). Preparation of ultrathin-shell double emulsions using the glass capillary microfluidic device was recorded by a CCD camera (IMX178, Sunny Optical Technology Co., Ltd, China). Scanning electron microscopy (SEM) images were obtained with a scanning electron microscope operated at an acceleration voltage of 3 kV (SU8010, Hitachi, Japan). SEM samples were freeze-dried in a freeze dryer (Shanghai Leewen Scientific Instruments, China). The diameters of the microcapsules were statistically measured using ImageJ software.

#### 2.5 Selective permeation and stimuli-triggered release of porous ultrathin-shell microcapsules

The shells of the porous ultrathin-shell microcapsules mainly consisted of shellac NPs cross-linked by telechelic  $\text{NH}_2\text{-PDMS-NH}_2$  molecules. Therefore, the shell was naturally porous. To test the permeation of the shell, molecules and NPs of different sizes, such as rhodamine B and rhodamine B-stained PLLA NPs, were encapsulated in the core. Rhodamine B molecules and rhodamine B-stained PLLA NPs have sizes of ~1 and 60 nm, respectively. Nile red was loaded in the shellac NPs, it was excited with a 488 nm laser and the resulting fluorescence (green) was observed from 500 to 520 nm. Rhodamine B was excited with a 543 nm laser and the fluorescence (red) was observed from 650 to 800 nm.

The release of cargos encapsulated in the porous ultrathin-shell microcapsules could be triggered by osmotic pressure or a pH change. To impose an osmotic pressure on the microcapsules, 50  $\text{mg}\cdot\text{mL}^{-1}$  PEG ( $M_w =$

6000  $\text{g}\cdot\text{mol}^{-1}$ ) was encapsulated in the microcapsules. When the outer aqueous phase containing 50  $\text{mg}\cdot\text{mL}^{-1}$  PEG was replaced by water, osmotic pressure was imposed on the microcapsules, and this led to swelling and rupture of the microcapsules. To change the pH, a small amount of 0.01  $\text{mol}\cdot\text{L}^{-1}$  NaOH solution was added to the outer aqueous phase, and the shellac NPs dissolved under the alkaline conditions, which resulted in disintegration of the microcapsules. The release processes triggered by osmotic pressure and pH changes were recorded with a CCD camera.

## 3 Results and Discussions

### 3.1 Preparation and characterization of ultrathin-shell microcapsules

To prepare porous ultrathin-shell microcapsules, ultrathin-shell double emulsions were used as templates, and the preparation and characterization of ultrathin-shell microcapsules are shown in Fig. 1. Ultrathin-shell W/O/W double emulsions were prepared by using a glass capillary microfluidic device, as schematically illustrated in Fig. 1(a). The inner aqueous phase comprising shellac NPs dispersed in water was sheared into droplets by the middle oil phase of  $\text{NH}_2\text{-PDMS-NH}_2$  dissolved in *n*-hexane. Subsequently, the dispersed droplets squeezed the middle oil phase into a thin layer at the second orifice, and both were sheared into ultrathin-shell W/O/W double emulsions by the outer aqueous phase, PVA, dissolved in water. To prepare the double emulsions, the flow rates of the inner, middle and outer phases were typically 200, 400, and 10000  $\mu\text{L}\cdot\text{h}^{-1}$ , respectively, and the shell thicknesses of the double emulsions were estimated to be ~383 nm (Fig. S1, cf. Electronic Supplementary material, ESM).

After preparation of the double emulsions, shellac NPs dispersed in the water core and telechelic  $\text{NH}_2\text{-PDMS-NH}_2$  molecules dissolved in the oil shell tended to complex electrostatically with each other over time at the water/oil interface, since the shellac NPs containing carboxylic groups were negatively charged and the telechelic  $\text{NH}_2\text{-PDMS-NH}_2$  molecules with amino groups were positively charged. Each telechelic  $\text{NH}_2\text{-PDMS-NH}_2$  molecule has two amino groups, and thus telechelic  $\text{NH}_2\text{-PDMS-NH}_2$  molecules bridged neighboring shellac NPs to form a cross-linked network. Additionally, *n*-hexane is volatile and gradually evaporated. Therefore, upon evaporation of the middle oil phase, ultrathin-shell double emulsions became porous ultrathin-shell microcapsules whose shells consisted of cross-linked networks of shellac NPs bridged by telechelic  $\text{NH}_2\text{-PDMS-NH}_2$  polymers, as schematically illustrated in Fig. 1(b).

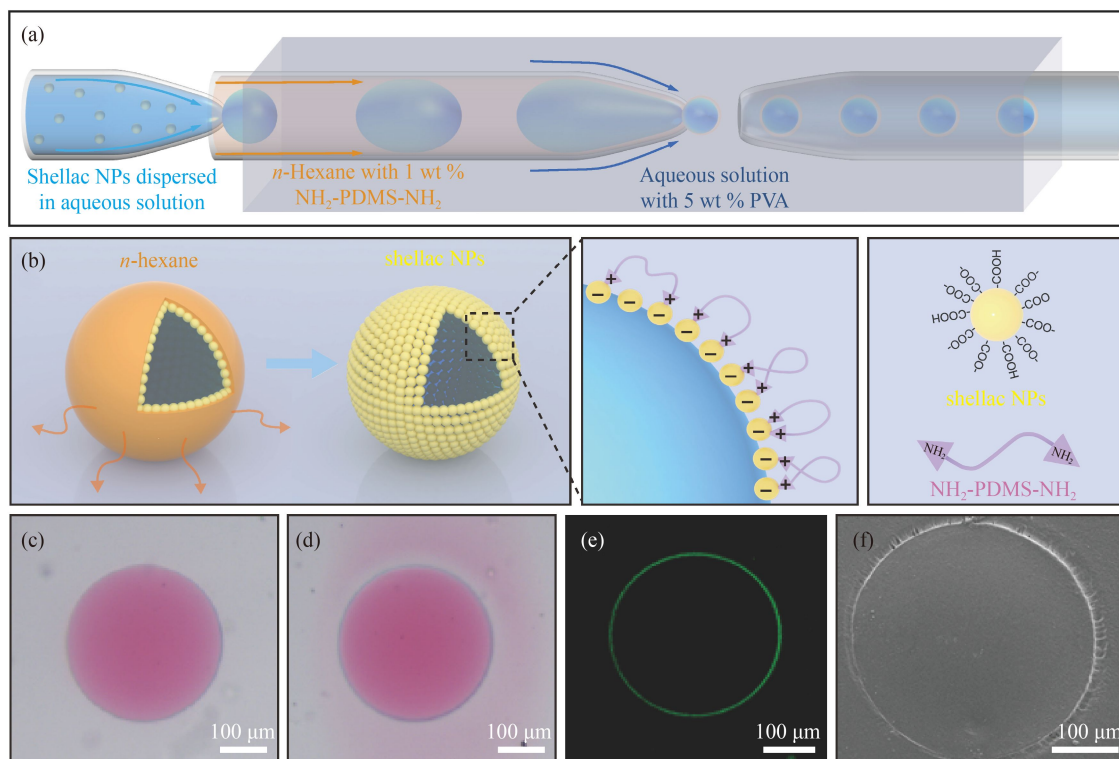


**Fig. 1** Design and preparation of porous ultrathin-shell microcapsules. (a) Schematic illustration of the preparation of ultrathin-shell W/O/W double emulsions using a glass capillary microfluidic device. Shellac NPs were dispersed in the inner water phase, and telechelic  $\text{NH}_2\text{-PDMS-NH}_2$  molecules were dissolved in the middle oil phase. (b) Negatively charged shellac NPs electrostatically complexed with positively charged telechelic polymers at the water/oil interface, and porous ultrathin-shell microcapsules were formed upon evaporation of the *n*-hexane. Since telechelic  $\text{NH}_2\text{-PDMS-NH}_2$  molecules possess two amino end groups, telechelic molecules were able to bridge neighboring shellac NPs, thus forming a cross-linked network. Optical microscope images of (c) ultrathin-shell double emulsions and (d) porous ultrathin-shell microcapsules. (e) Fluorescent confocal microscope image of a porous ultrathin-shell microcapsule with Nile red loaded in the shellac NPs. (f) SEM image of a collapsed porous ultrathin-shell microcapsule.

To better visualize the water core, red ink was dissolved in the inner aqueous phase. When the ultrathin-shell double emulsions were first prepared, red ink could not diffuse across the oil shell and was confined within the core, as shown in Fig. 1(c). However, when the oil phase was evaporated and ultrathin-shell double emulsions became porous ultrathin-shell microcapsules, red ink diffused out of the microcapsules, as shown in Fig. 1(d). The porous ultrathin shell was directly visualized by loading Nile red into the shellac NPs, which shows a thin fluorescent ring under a fluorescence confocal microscope (Fig. 1(e)). A SEM photograph that when the ultrathin-shell microcapsule was dried, its shell collapsed and flattened with only a small wrinkle around the microcapsule edge, as shown in Fig. 1(f).

### 3.2 Tuning the size of ultrathin-shell W/O/W double emulsions

Since porous ultrathin-shell microcapsules were templated from ultrathin-shell W/O/W double emulsions, the size of the microcapsules could be tailored by tuning the size of the double emulsions, as shown in Fig. 2.

When the flow rates of the middle and outer phases were fixed at  $800$  and  $10000 \mu\text{L}\cdot\text{h}^{-1}$ , respectively, ultrathin-shell double emulsions were generated stably, with their sizes decrease slightly from  $370 \mu\text{m}$  to  $350 \mu\text{m}$  as the inner phase flow rate was increased from  $200$  to  $600 \mu\text{L}\cdot\text{h}^{-1}$ , as shown in Fig. 2(a). In contrast, the emulsion sizes increase slightly from  $330 \mu\text{m}$  to  $365 \mu\text{m}$  when the middle phase flow rate was increased from  $200$  to  $1000 \mu\text{L}\cdot\text{h}^{-1}$ , while the flow rates of the inner and outer phases were fixed at  $200$  and  $10000 \mu\text{L}\cdot\text{h}^{-1}$ , respectively, as shown in Fig. 2(b). When the flow rates of the inner and middle phases were kept constant at  $200$  and  $800 \mu\text{L}\cdot\text{h}^{-1}$ , respectively, the emulsion sizes decrease from  $365 \mu\text{m}$  to  $305 \mu\text{m}$  as the outer phase flow rate was increased from  $10000$  to  $18000 \mu\text{L}\cdot\text{h}^{-1}$ , as shown in Fig. 2(c). When the flow rates of the inner, middle and outer phases continued to increase beyond  $600$ ,  $1000$ , and  $18000 \mu\text{L}\cdot\text{h}^{-1}$ , respectively, stable ultrathin-shell double emulsions were not formed. Overall, the flow rates of the inner and middle phases only have a limited effect on the emulsion size. In contrast, the outer aqueous phase is able to shear the double emulsion into smaller size as its flow rate increases.

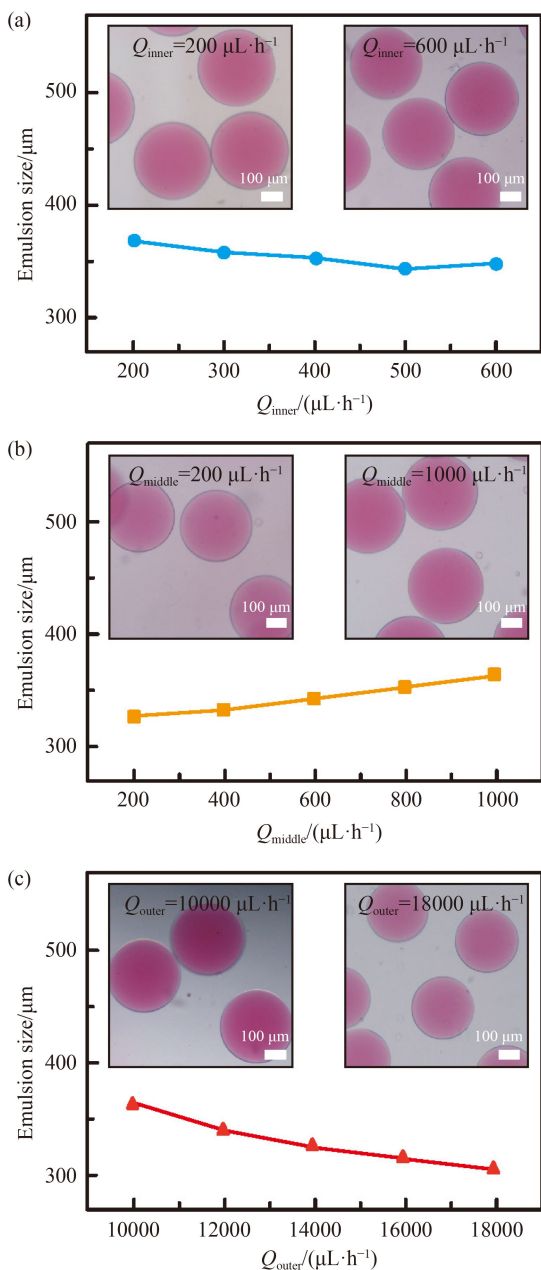


**Fig. 2** Tuning the size of ultrathin-shell W/O/W double emulsions, which were used as templates for preparation of porous ultrathin-shell microcapsules. (a) Dependence of the emulsion size on the inner phase flow rate. The flow rates of the middle and outer phases were fixed at 800 and 10000  $\mu\text{L}\cdot\text{h}^{-1}$ , respectively. (b) Dependence of the emulsion size on the middle phase flow rate. The flow rates of the inner and outer phases were kept constant at 200 and 10000  $\mu\text{L}\cdot\text{h}^{-1}$ , respectively. (c) Dependence of the emulsion size on the outer phase flow rate. The flow rates of the inner and middle phases were kept constant at 200 and 800  $\mu\text{L}\cdot\text{h}^{-1}$ , respectively. Red ink was dissolved in the inner phase for better visualization.

### 3.3 Selective permeation of porous ultrathin-shell microcapsules

The shells of microcapsules consist of cross-linked

networks of shellac NPs bridged by telechelic polymers, and thus the microcapsules are naturally porous, which might allow selective permeation of particles with different sizes, as shown in Fig. 3. The size of the shellac NPs is  $D \approx 100$  nm. If they are assumed to be densely packed, the pores between shellac NPs are estimated to be  $\sim 20$  nm, as illustrated schematically in Fig. 3(a). To explore permeation of the porous ultrathin-shell microcapsules, rhodamine B with a size of  $\sim 1$  nm and rhodamine B-stained PLLA NPs with size of  $\sim 60$  nm were encapsulated in the cores of the microcapsules. Because rhodamine B molecules are smaller than the pores on the shell, rhodamine B molecules were able to diffuse out of the microcapsules, resulting in a red fluorescent color both inside and outside the microcapsules, as shown in Fig. 3(b). However, the rhodamine B-stained PLLA NPs are larger than the pores, and they were stably encapsulated within the core; therefore, the red fluorescent color of rhodamine B was only observed within the microcapsules, as shown in Fig. 3(c). Selective permeation of porous microcapsules differs from most microcapsules with solid shells and is especially useful for applications that require encapsulation of large molecules inside the core and transport of small molecules across the shell [29,30].

### 3.4 Stimuli-triggered release of porous ultrathin-shell microcapsules

After preparation, porous ultrathin-shell microcapsules were stable for long periods of time. To release the cargos encapsulated in the core, the microcapsules could be ruptured by osmotic pressure or disintegrated under a pH change, showing osmotic pressure-triggered or pH-triggered releases, as shown in Fig. 4. To impose an osmotic pressure on the microcapsules, 50  $\text{mg}\cdot\text{mL}^{-1}$  PEG with an  $M_w$  of 6000  $\text{g}\cdot\text{mol}^{-1}$  was added into the inner and outer aqueous phases. The gyration radius of PEG was estimated to be  $\sim 3.1$  nm (cf. ESM) [31]. When the outer aqueous phase was replaced by water, the high concentration of PEG in the inner generated high osmotic pressures inside the microcapsules [32], thus leading to swelling and eventually rupture of the microcapsules. Interestingly, after rupture, the shells shrank, since they consisted of cross-linked networks of shellac NPs formed by telechelic polymers, as shown in Figs. 4(a) and 4(b). Alternatively, to trigger release of the cargo via pH change, NaOH solution was added into the continuous phase. Under alkaline condition, more carboxylic groups were deprotonated, and the shellac became soluble in the aqueous solution, thus leading to disintegration of the microcapsules; this was confirmed by optical microscopy, as shown in Figs. 4(c) and 4(d). Although the osmotic pressure-triggered and pH-triggered releases have different underlying mechanisms, both of them could release the cargo quickly and could be applied under

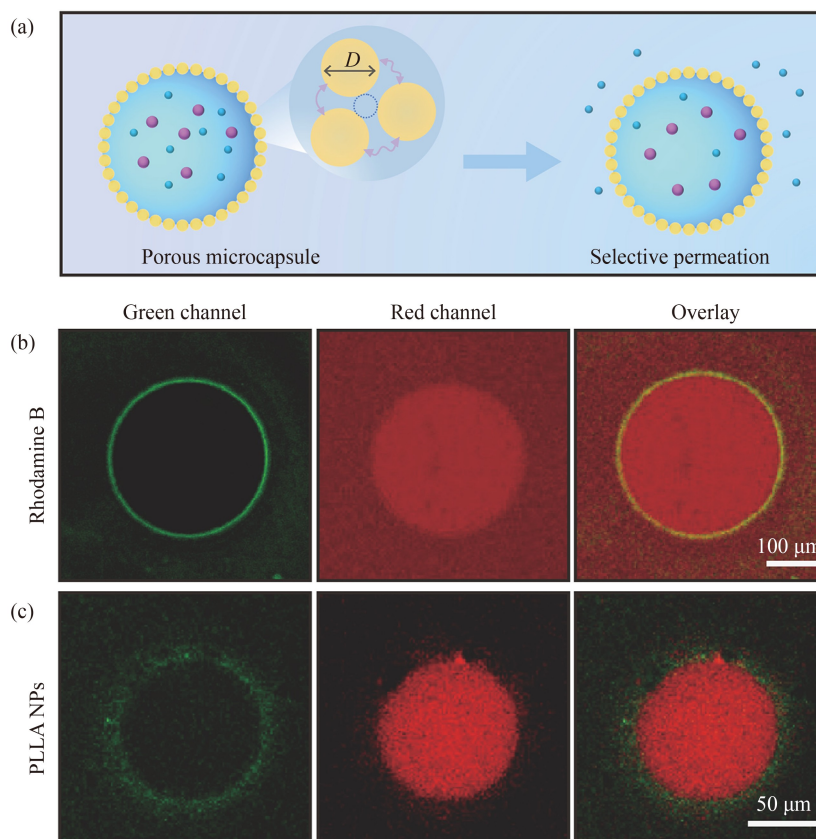


**Fig. 3** Selective permeation of porous ultrathin-shell microcapsules. (a) Schematic illustration of selective permeation of small molecules or particles across the porous ultrathin shell. Fluorescence confocal microscope images of (b) rhodamine B molecules with size of ~1 nm and (c) rhodamine B-stained PLLA NPs with size of ~60 nm encapsulated in the porous ultrathin-shell microcapsules. Nile red was loaded in shellac NPs, and its fluorescent color (green) was excited by a 488 nm laser and observed between 500 nm and 520 nm. The fluorescent color (red) of rhodamine B was excited by a 543 nm laser and observed between 650 and 800 nm.

suitable conditions.

Porous ultrathin-shell microcapsules are unique and have several advantages. The porous shell allows encapsulation of large molecules or particles in the cores and permeation of small molecules or particles across the shells. Because of the ultrathin shells, cargos encapsulated in the microcapsules could be released when triggered by osmotic pressure. In addition, the shell comprising a network of shellac NPs cross-linked by telechelic polymers could be destroyed by dissolving the shellac NPs under alkaline condition. For traditional microcapsules with solid shells, it is generally difficult to achieve selective permeation, and the prepared microcapsules show superior size-dependent permeation and multiple stimuli-triggered release modes.

## 4 Conclusions

In summary, porous ultrathin-shell microcapsules were designed and prepared by using ultrathin-shell W/O/W double emulsions as templates. The microcapsules consisted of ultrathin shells comprising a network of

negatively charged shellac NPs crosslinked by positively charged telechelic polymers and are naturally porous, thus enabling encapsulation of large molecules or particles in the core and permeation of small molecules or nanoparticles across the shell. The cargos encapsulated in the microcapsules could be released when triggered by osmotic pressure or a pH change. Overall, this study presents a novel strategy for designing porous ultrathin-shell microcapsules, and the diverse functions of the prepared microcapsules suggest that they have promise for applications requiring size-dependent permeation and stimuli-triggered release, such as in biomedicine and drug delivery.

**Acknowledgments** This work is supported by National Key Research and Development Program of China (Grant Nos. YS2021YFC3000089, 2020YFA0908200), Zhejiang Provincial Natural Science Foundation of China (Grant No. Y20B060027), National Natural Science Foundation of China (Grant No. 21878258), ARC Discovery Project (Grant Nos. DP200101238, DP210103079), and NHMRC Investigator Grant APP2008698.

**Electronic Supplementary Material** Supplementary material is available in the online version of this article at <https://dx.doi.org/10.1007/s11705-022-2201-z> and is accessible for authorized users.

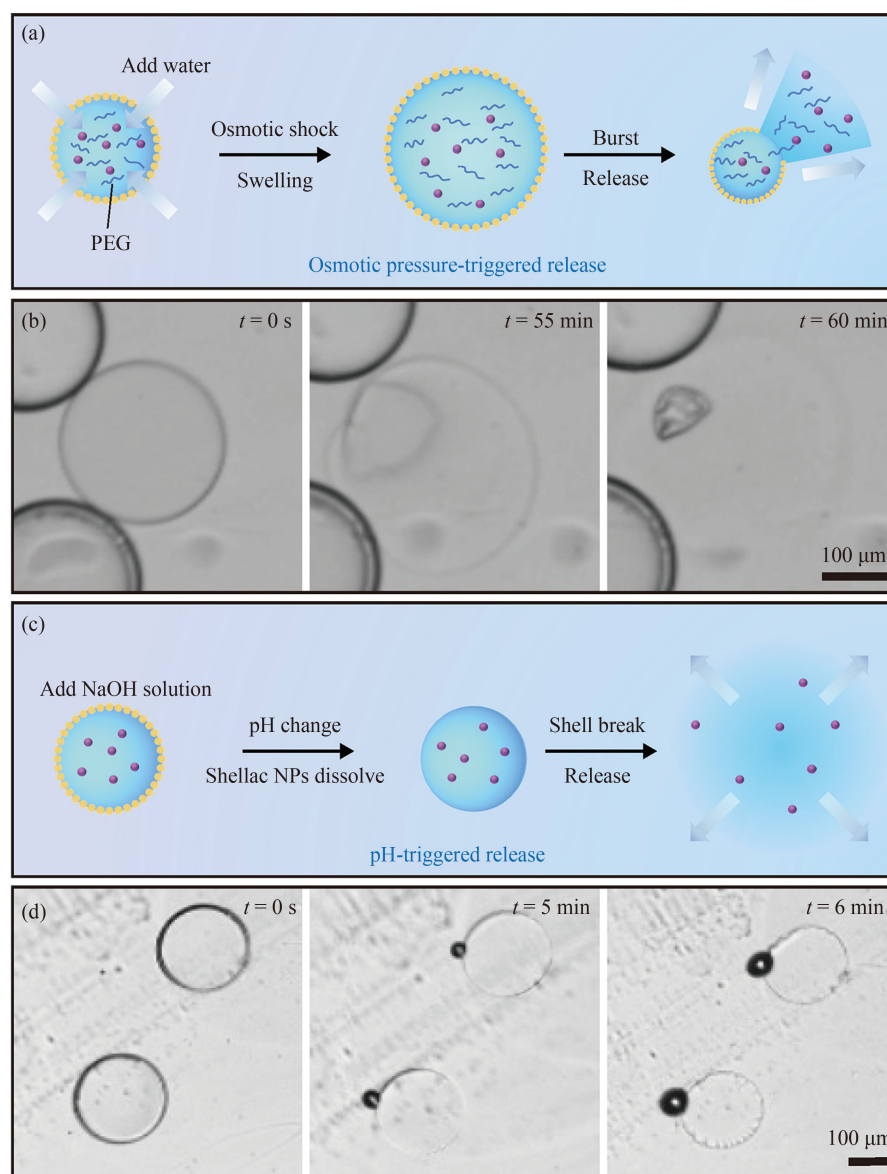


**Fig. 4** Stimuli-triggered release of porous ultrathin-shell microcapsules. (a) Schematic illustration of osmotic pressure-triggered release. (b) Sequences of snapshots showing swelling and rupture of the porous ultrathin-shell microcapsules triggered by osmotic pressure. The microcapsules contained  $50 \text{ mg}\cdot\text{mL}^{-1}$  PEG in the core, and water was added to the continuous phase to impose an osmotic pressure. (c) Schematic illustration of pH-triggered release. (d) Sequences of snapshots showing disintegration of the porous ultrathin-shell microcapsules under alkaline condition. NaOH solution was added to the continuous phase, and shellac NPs were dissolved after the pH change, leading to disintegration of the microcapsules.

## References

- Lee H, Choi C H, Abbaspourrad A, Wesner C, Caggioni M, Zhu T, Weitz D A. Encapsulation and enhanced retention of fragrance in polymer microcapsules. *ACS Applied Materials & Interfaces*, 2016, 8(6): 4007–4013
- Nam C, Yoon J, Ryu S A, Choi C H, Lee H. Water and oil insoluble PEGDA-based microcapsule: biocompatible and multicomponent encapsulation. *ACS Applied Materials & Interfaces*, 2018, 10(47): 40366–40371
- Chu J O, Choi Y, Kim D W, Jeong H S, Park J P, Weitz D A, Lee S J, Lee H, Choi C H. Cell-inspired hydrogel microcapsules with a thin oil layer for enhanced retention of highly reactive antioxidants. *ACS Applied Materials & Interfaces*, 2022, 14(2): 2597–2604
- Ling S D, Geng Y, Chen A, Du Y, Xu J. Enhanced single-cell encapsulation in microfluidic devices: from droplet generation to single-cell analysis. *Biomicrofluidics*, 2020, 14(6): 61508
- Pessi J, Santos H A, Miroshnyk I, JoukoYliruusi, Weitz D A, Mirza S. Microfluidics-assisted engineering of polymeric microcapsules with high encapsulation efficiency for protein drug delivery. *International Journal of Pharmaceutics*, 2014, 472(1): 82–87
- Choi C H, Lee H, Abbaspourrad A, Kim J H, Fan J, Caggioni M, Wesner C, Zhu T, Weitz D A. Triple emulsion drops with an

- ultrathin water layer: high encapsulation efficiency and enhanced cargo retention in microcapsules. *Advanced Materials*, 2016, 28(17): 3340–3344
7. Zhu P, Kong T, Tang X, Wang L. Well-defined porous membranes for robust omniphobic surfaces via microfluidic emulsion templating. *Nature Communications*, 2017, 8(1): 15823
  8. Chen L, Xiao Y, Wu Q, Yan X, Zhao P, Ruan J, Shan J, Chen D, Weitz D A, Ye F. Emulsion designer using microfluidic three-dimensional droplet printing in droplet. *Small*, 2021, 17(39): 2102579
  9. Sobczak G, Wojciechowski T, Sashuk V. Submicron colloidosomes of tunable size and wall thickness. *Langmuir*, 2017, 33(7): 1725–1731
  10. Wu S, Xin Z, Zhao S, Sun S. High-throughput droplet microfluidic synthesis of hierarchical metal–organic framework nanosheet microcapsules. *Nano Research*, 2019, 12(11): 2736–2742
  11. Hitchcock J P, Tasker A L, Baxter E A, Biggs S, Cayre O J. Long-term retention of small, volatile molecular species within metallic microcapsules. *ACS Applied Materials & Interfaces*, 2015, 7(27): 14808–14815
  12. Zhang M J, Zhang P, Qiu L D, Chen T, Wang W, Chu L Y. Controllable microfluidic fabrication of microstructured functional materials. *Biomicrofluidics*, 2020, 14(6): 061501
  13. He F, Wang W, He X H, Yang X L, Li M, Xie R, Ju X J, Liu Z, Chu L Y. Controllable multicompartmental capsules with distinct cores and shells for synergistic release. *ACS Applied Materials & Interfaces*, 2016, 8(13): 8743–8754
  14. You X R, Ju X J, He F, Wang Y, Liu Z, Wang W, Chu L Y. Polymersomes with rapid K(+)-triggered drug-release behaviors. *ACS Applied Materials & Interfaces*, 2017, 9(22): 19258–19268
  15. Geryak R, Quigley E, Kim S, Korolovych V F, Calabrese R, Kaplan D L, Tsukruk V V. Tunable interfacial properties in silk ionomer microcapsules with tailored multilayer interactions. *Macromolecular Bioscience*, 2019, 19(3): 1800176
  16. Tian T, Ruan J, Zhang J, Zhao C X, Chen D, Shan J. Nanocarrier-based tumor-targeting drug delivery systems for hepatocellular carcinoma treatments: enhanced therapeutic efficacy and reduced drug toxicity. *Journal of Biomedical Nanotechnology*, 2022, 18(3): 660–676
  17. Xie X, Zhang W, Abbaspourad A, Ahn J, Bader A, Bose S, Vegas A, Lin J, Tao J, Hang T, Lee H, Iverson N, Bisker G, Li L, Strano M S, Weitz D A, Anderson D G. Microfluidic fabrication of colloidal nanomaterials-encapsulated microcapsules for biomolecular sensing. *Nano Letters*, 2017, 17(3): 2015–2020
  18. Sun H, Zheng H, Tang Q, Dong Y, Qu F, Wang Y, Yang G, Meng T. Monodisperse alginate microcapsules with spatially confined bioactive molecules via microfluid-generated W/W/O emulsions. *ACS Applied Materials & Interfaces*, 2019, 11(40): 37313–37321
  19. Polenz I, Datta S S, Weitz D A. Controlling the morphology of polyurea microcapsules using microfluidics. *Langmuir*, 2014, 30(40): 13405–13410
  20. Sun Z, Yang C, Eggersdorfer M, Cui J, Li Y, Hai M, Chen D, Weitz D A. A general strategy for one-step fabrication of biocompatible microcapsules with controlled active release. *Chinese Chemical Letters*, 2020, 31(1): 249–252
  21. Liu Z, Ju X J, Wang W, Xie R, Jiang L, Chen Q, Zhang Y Q, Wu J F, Chu L Y. Stimuli-responsive capsule membranes for controlled release in pharmaceutical applications. *Current Pharmaceutical Design*, 2017, 23(2): 295–301
  22. Chen L, Yang C, Xiao Y, Yan X, Hu L, Eggersdorfer M, Chen D, Weitz D A, Ye F. Millifluidics, microfluidics, and nanofluidics: manipulating fluids at varying length scales. *Materials Today Nano*, 2021, 16: 100136
  23. Sun Z, Yan X, Xiao Y, Hu L, Eggersdorfer M, Chen D, Yang Z, Weitz D A. Pickering emulsions stabilized by colloidal surfactants: role of solid particles. *Particuology*, 2022, 64: 153–163
  24. Choi Y H, Hwang J, Han S H, Lee C, Jeon S, Kim S. Thermo-responsive microcapsules with tunable molecular permeability for controlled encapsulation and release. *Advanced Functional Materials*, 2021, 31(24): 2100782
  25. Lee T Y, Ku M, Kim B, Lee S, Yang J, Kim S H. Microfluidic production of biodegradable microcapsules for sustained release of hydrophilic actives. *Small*, 2017, 13(29): 1700646
  26. Perrotton J, Ahijado-Guzmán R, Moleiro L H, Tinao B, Guerrero-Martinez A, Amstad E, Monroy F, Arriaga L R. Microfluidic fabrication of vesicles with hybrid lipid/nanoparticle bilayer membranes. *Soft Matter*, 2019, 15(6): 1388–1395
  27. Wu B, Yang C, Xin Q, Kong L, Eggersdorfer M, Ruan J, Zhao P, Shan J, Liu K, Chen D, Weitz D A, Gao X. Attractive Pickering emulsion gels. *Advanced Materials*, 2021, 33(33): 2102362
  28. Yan X, Wu B, Wu Q, Chen L, Ye F, Chen D. Interfacial engineering of attractive Pickering emulsion gel-templated porous materials for enhanced solar vapor generation. *Energies*, 2021, 14(19): 6077
  29. Luo G, Yu Y, Yuan Y, Chen X, Liu Z, Kong T. Freeform, reconfigurable embedded printing of all-aqueous 3D architectures. *Advanced Materials*, 2019, 31(49): 1904631
  30. Werner J G, Weitz D A, Lee H, Wiesner U. Ordered mesoporous microcapsules from double emulsion confined block copolymer self-assembly. *ACS Nano*, 2021, 15(2): 3490–3499
  31. Thierry B, Griesser H J. Dense PEG layers for efficient immunotargeting of nanoparticles to cancer cells. *Journal of Materials Chemistry*, 2012, 22(18): 8810
  32. Schiller L R, Emmett M, Santa Ana C A, Fordtran J S. Osmotic effects of polyethylene glycol. *Gastroenterology*, 1988, 94(4): 933–941